Spiral State and Giant Magnetoresistance in Perovskite Mn Oxides

J. Inoue and S. Maekawa
Department of Applied Physics, Nagoya University, Nagoya 464-01, Japan
(Received 13 December 1994)

A spiral state is proposed to be the stable magnetic structure of perovskite (La-X)MnO_3 (X: Ba, Ca, or Sr) with a low concentration of X ions, contrary to the canted state predicted before. We use a mean field approximation applied to a model which treats t_{2g} and e_g electrons of Mn ions as localized spins and strongly correlated itinerant electrons, respectively, and includes a strong Hund coupling between them. We find that the Hund coupling is crucial for the giant magnetoresistance observed in (La-X)MnO_3, indicating that the Hund coupling enhances the dependence of the resistivity on the induced magnetization in agreement with experiments.

PACS numbers: 71.27.+a, 72.15.Gd, 75.10.–b

Perovskite Mn oxides, $(La_{1-x}X_x)MnO_3$ with X = Ba, Ca, Sr, etc. have recently attracted considerable attention because of a huge negative magnetoresistance (giant magnetoresistance or GMR) near room temperature [1–7]. The resistivity drop due to an external magnetic field is usually much larger than that observed in magnetic multilayers [8]. Indeed, the resistivity in (Pr-Ca)MnO_3 reaches 10^{-6} times smaller than that without the magnetic field [9]. This is actually an insulator-metal transition caused by the magnetic field. The GMR in (La-X)MnO_3 is important not only for the basic physics of strong electron correlations, but for technical applications, because the temperature at which the GMR occurs can be controlled by tuning the carrier numbers. The transition metal oxides are systems with strong electron correlations and show a rich variety of physical phenomena [10,11]. Among them, $(La_{1-x}X_x)MnO_3$ are well-known materials in which an antiferromagnetic insulating phase at $x = 0$ changes to a metallic ferromagnetism for $0.2 \lesssim x \lesssim 0.5$ [12]. A competition between the kinetic and exchange energies has led to the prediction of the existence of the canted ferromagnetism for $0 < x < 0.2$ [13]. However, no clear evidence of the canted ferromagnetism has yet been reported especially by microscopic measurements such as neutron diffraction experiments. This is in contrast with observations for, e.g., $(La\text{-}Sr)_2CuO_4$ [14] and $V_{2-\delta}O_3$ [15], where the antiferromagnetic insulating phase caused by the strong electron correlations changes to an incommensurate antiferromagnetism on doping of holes. Thus both the magnetic and transport properties in the Mn oxides are left to be explained from the viewpoint of strong electron correlations.

In this Letter, we study the magnetic phase diagram and the origin of the GMR in (La-X)MnO_3 using a model where correlated itinerant electrons and localized spins coexist and a strong Hund coupling between them exists. By making use of a mean field approximation, we will show that a spiral state becomes stable for small-x regions on doping of holes in contrast to the canted state predicted many years ago [13] and accepted since then. The spiral state changes continuously to the ferromagnetic state, and the canted state appears at concentrations with x close to 1.0. The dependence of the electrical resistivity on the magnetic field is studied in the strong coupling limit of the model. The strong Hund coupling is shown to enhance the magnetoresistance effect, leading to a qualitative explanation of the experimental observations [7].

The appearance of metallic ferromagnetism on doping has been explained by the mechanism of the double exchange interaction [16,17]. The Mn^{3+} ions in $LaMnO_3$ have three electrons in the t_{2g} state and one electron in the e_g state due to the Hund coupling. Because of the strong Hund coupling and on-site Coulomb repulsion between e_g electrons, $LaMnO_3$ is an antiferromagnetic insulator. On replacing La atoms with X (Ba, Ca, or Sr) atoms, Mn ions change to the Mn^{4+} state without e_g electrons. The vacant e_g state of Mn^{4+} makes it possible for e_g electrons in surrounding Mn^{3+} ions to hop into the e_g state of Mn^{4+} so long as the t_{2g} spins of the neighboring Mn^{3+} and Mn^{4+} ions are parallel. Thus a competition appears between a gain in the kinetic energy and a loss in the exchange energy of t_{2g} spins which favor antiferromagnetic coupling. With increasing number of mobile carriers on further doping of X atoms, the gain in the kinetic energy overcomes the loss of the exchange energy, which results in a transition to metallic ferromagnetism around $x \sim 0.2$.

We consider only Mn ions, disregarding the other kinds of atoms, La, O, etc. The role of these atoms may be implicitly included in the parameter values in the model. We treat t_{2g} and e_g electrons of Mn ions as localized spins of $S = 3/2$ and itinerant electrons of $S = 1/2$, respectively. The treatment for t_{2g} electrons may be justified by the small overlap between t_{2g} wave functions and oxygen p states and by the fact that $XMnO_3$ is also an antiferromagnetic insulator with a Néel temperature of $\sim$120 K [12]. The localized spins couple antiferromagnetically with each other and the strong Hund coupling acts between the localized spins and spins of itinerant electrons. Because of the ionic character of the material, there exist strong electron correlations among the itinerant electrons. Thus the Hamilton-

ian is given by

$$H = -t\sum_{ij\sigma} a^{\dagger}_{i\sigma}a_{j\sigma} + \sum_{i\sigma}\epsilon_0 a^{\dagger}_{i\sigma}a_{i\sigma} + U\sum_i n_{i\uparrow}n_{i\downarrow} + J\sum_{\langle ij\rangle}\mathbf{S}_i\cdot\mathbf{S}_j - \frac{K}{2}\sum_i \mathbf{S}_i\cdot\sigma_i . \quad (1)$$

Here, t (>0) denotes the transfer integral of itinerant electrons between nearest-neighbor (NN) sites, ϵ_0 the on-site potential of itinerant electrons, U the on-site Coulomb repulsion between $\uparrow$ and $\downarrow$ spin itinerant electrons, $a^{\dagger}_{i\sigma}$ ($a_{i\sigma}$) is a creation (an annihilation) operator of an itinerant electron at site i with spin σ, $n_{i\sigma} = a^{\dagger}_{i\sigma}a_{i\sigma}$, J (>0) is the NN exchange interaction between localized spins, K (>0) represents the Hund coupling, and $\boldsymbol{\sigma}$ stands for the Pauli matrix.

We apply the Hartree-Fock approximation to the Hamiltonian and survey the magnetic phase diagram of $(La_{1-x}X_x)MnO_3$ comparing the free energies of the ferromagnetic (F), collinear antiferromagnetic (AF), canted (CN), and (1,1,1) spiral (SP) states. Illustrations for one-dimensional SP and CN states are shown in Figs. 1(a) and 1(b), respectively.

By using a local spin quantization axis, the one-electron eigenvalues for the (1,1,1) SP state with a propagation wave vector $\pi + 2\theta$ and the CN state with two sublattices (canting angle 2θ) are given by

$$E^{\mathrm{SP}}_{\mathbf{k}} = v_0 - \epsilon_{\mathbf{k}}\sin\theta \pm \{\Delta_E^2 + \epsilon'^2_{\mathbf{k}}\cos^2\theta\}^{1/2}, \quad (2)$$

$$E^{\mathrm{CN}}_{\mathbf{k}} = v_0 \pm \{\Delta_E^2 + \epsilon^2_{\mathbf{k}} \pm \Delta_E\epsilon_{\mathbf{k}}\sin\theta\}^{1/2}, \quad (3)$$

respectively. Here, $\epsilon_{\mathbf{k}} = -2t\sum_{\gamma=1}^{d}\cos k_\gamma$, $\epsilon'_{\mathbf{k}} = 2t\sum_{\gamma=1}^{d}\sin k_\gamma$, where d denotes the dimensionality ($d = 3$ in this case), Δ_E is the effective field, and v_0 is the normalized on-site potential . The results are valid also for two-dimensional (1,1) SP and CN states as well as for one-dimensional states. The eigenvalues of AF and F states are correctly obtained in the limits of $\theta = 0$ and $\theta = \pi/2$, respectively. Illustrations of $E^{\mathrm{SP}}_{\mathbf{k}}$ and $E^{\mathrm{CN}}_{\mathbf{k}}$ are shown in Figs. 2(a) and 2(b), respectively, for the one-dimensional case with $\Delta_E = 2.5t$. The wave vector is measured in units of the lattice constant. In Fig. 2(a), the wave vector is shifted by $\pi/2$ in order to make the comparison between $E^{\mathrm{SP}}_{\mathbf{k}}$ and $E^{\mathrm{CN}}_{\mathbf{k}}$ easy.

The free energy of the itinerant electrons per site is calculated for the lowest order of the carrier density δ, which is the number of holes when x is small or the number of electrons near low density when x is large. The states near $x \sim 0$ correspond to those near half filling in the one-band Hubbard model. By assuming that $\Delta_E > 2dt$, which corresponds to the case of large Hund coupling, the free energy of the itinerant electrons is given by the product of δ and the band edge of the lower energy branch occupied by the carriers. The free energy of the localized spins is calculated in the usual way.

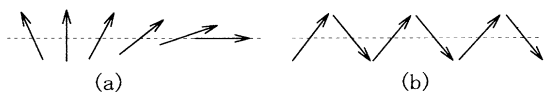

FIG. 1. Schematic figures of one-dimensional (a) spiral (SP) and (b) canted (CN) states.

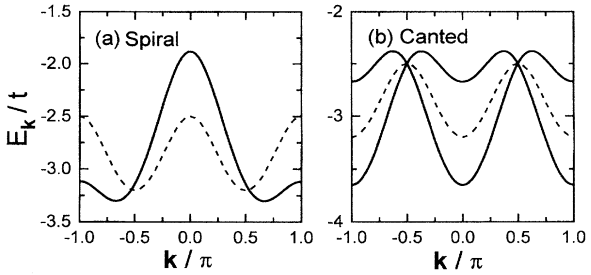

FIG. 2. Calculated results of the lower half of the energy eigenvalues $E_{\mathbf{k}}$ for (a) spiral and (b) canted states along the symmetrical line of wave vector $\mathbf{k}$. Upper halves are not shown here. Dashed curves are $E_{\mathbf{k}}$ for the antiferromagnetic state. There are two branches of $E_{\mathbf{k}}$ for the canted state because of the two sublattice structure.

By minimizing the total free energy with respect to θ with fixed δ, we obtain the phase diagram. Phase diagrams at zero temperature are shown in Figs. 3(a) and 3(b) for near half filling ($x \sim 0$) and at low density ($x \sim 1$), respectively. Near half filling, the AF state at $\delta = 0$ changes to the SP state with δ and continuously changes to the F state for $\delta > 2JS^2/t$. The angle θ in the SP state is given by $\sin\theta = \delta t/2JS^2$. As the angle between NN spins is $|\pi \pm 2\theta|$, θ is about 0.3π for $\delta = 0.2$, $J/t = 0.05$, and $S = 3/2$, and it is reduced to 0.13π with a slightly increased value of $\delta = 0.22$. At low density, the AF state at $\delta = 0$ changes to the CN state with δ and becomes the F state continuously for $\delta > (JS^2/t)2(1 + 2dt/\Delta_E)$. The canting angle θ in this case is approximately given by $\sin\theta \sim \Delta_E^2\delta/2JS^2(\Delta_E^2 + 4d^2t^2)^{1/2}$ for small θ.

The physical reason for the appearance of SP and CN states near half filling and at low density, respectively, may be explained as follows. As shown in Figs. 2(a) and 2(b), the electronic structures are greatly distorted near $\mathbf{k} = (0,0,0)$ for the CN state and $(\pi/2, \pi/2, \pi/2)$ for the SP state with increasing angle θ. As the electrons are filled around $\mathbf{k} = (0,0,0)$ at low density, it is favorable for the CN state to gain the kinetic energy by changing

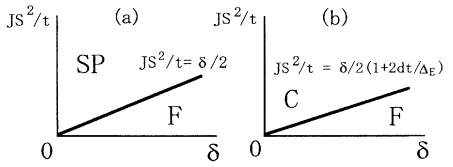

FIG. 3. Magnetic phase diagrams (δ vs JS^2/t) at zero temperature for the (a) spiral and (b) canted states.

the electronic structure around $\mathbf{k} = (0,0,0)$. In contrast, near half filling, it becomes favorable for the SP state to gain the kinetic energy because the carriers (holes) are filled around $\mathbf{k} = (\pi/2, \pi/2, \pi/2)$. A more intuitive explanation can be given as follows. The change from the AF state to the CN state is nothing but the appearance of a uniform component in the magnetic structure, which is correlated with a change in electronic structures with small wave vectors. On the other hand, the change from the AF state to the SP state is correlated with a change in electronic structures with large wave vectors.

The T-x phase diagram for $(La_{1-x}X_x)MnO_3$ at low temperatures is shown in Fig. 4. The SP state is stable in the region close to half filling, i.e., $x \sim 0$, the CN state is stable near $x \sim 1$, and the F state becomes most stable in the intermediate concentrations. The present result, in which the AF state changes into the SP state, is consistent with the theoretical result that the AF insulating phase at half filling in the Hubbard model or t-J model changes to the spiral state on doping of holes [18,19].

The approach to the GMR in these systems is based on the concept of strong electron correlations discussed in the one-band Hubbard model by Brinkman and Rice [20] and Ohata and Kubo [21]. We generalize the moment method [21] to the strong coupling limit of the present model where both U and K in Eq. (1) tend to infinity. In this case, the Hamiltonian for itinerant electrons can be expressed as $\mathcal{H} = -t\sum_{ij,\sigma} \tilde{c}^{\dagger}_{i\sigma}\tilde{c}_{j\sigma}$, where $\tilde{c}^{\dagger}_{i\sigma}(\tilde{c}_{i\sigma})$ is a creation (annihilation) operator projecting out both the double occupancy of the itinerant electrons and an antiparallel alignment of the localized and itinerant spins on the same site.

The frequency-dependent conductivity can be written as

$$\sigma_{xx}(\omega) = \frac{1}{\Omega}\int_0^{\infty} dt\, e^{i\omega t}\int_0^{\beta} d\lambda \langle J_x(-i\lambda)J_x(t)\rangle, \quad (4)$$

with a current operator J_x, $\beta = 1/k_BT$, and the volume Ω. It has been shown that the line shape of $\sigma_{xx}(\omega)$ can be obtained from its second and fourth moments m_2 and m_4. It is Gaussian when $\xi \equiv m_4/3m_2^2 \sim 1$ and Lorentzian when $\xi \gg 1$ [21]. The resistivity ρ is defined as the inverse of the diffusion constant D, $\rho = D^{-1}$, and D is related to the static conductivity σ_{xx} by $\sigma_{xx} = Ne^2D/k_BT\Omega$. The moments are evaluated as functions of concentration c of up (or down) spin sites at high temperature for a single mobile carrier in the half-filled state corresponding to $x = 0$. After counting the number of paths contributing to m_2 and m_4, we can show that $\xi = 1$ for $c = 0.5$ and that the line shape of $\phi(t)$ is Gaussian, while it is Lorentzian for $c \sim 1$ as $\xi \to \infty$ in this case. When c is close to 0.5, that is, the spin arrangement is almost random, the resistivity is calculated as

$$\rho = \frac{1}{a^2t^2}\frac{1}{1-2c(1-c)}\sqrt{\frac{m_2}{2\pi}} \sim \sqrt{\frac{8}{\pi}}\frac{1-7p^2}{a^2t}, \quad (5)$$

where a is the lattice constant and $p \equiv 0.5 - c$. Noting that the difference between the number of up and down spin sites is proportional to the net magnetization M, i.e., $2p = M/M_s$ with the saturation magnetization M_s, Eq. (5) can be rewritten as

$$\rho = \rho_0\{1 - A(M/M_s)^2\}. \quad (6)$$

Here, ρ_0 is the resistivity for $M = 0$. In the present model, the coefficient A is $7/4$, while it is $1/2$ in the one-band Hubbard model. Furthermore, the value of ρ_0 is larger in the present model than that in the Hubbard model by a factor $2\sqrt{2/3}$ as expected. The increase of the value of A is due to the restriction of the motion of mobile carriers by the strong Hund coupling as interpreted below.

In the strong coupling limit of the Hubbard model, where double occupancy of each site is prohibited, there are two types of paths contributing to the moments. One is a closed path and the other is a retraceable path. The number of paths of the former type is limited because of the restriction that the initial states must be the same as the final state after the hopping of the mobile carrier, while the paths of the latter type are always permitted because the mobile carrier can go and come back always on the same path without disturbing the background spin states. In the present model, however, there appears another restriction due to the strong Hund coupling; that is, the mobile carrier can hop only to sites where the localized spins are parallel to the spin of the mobile carrier. Therefore, the paths which contribute to the moments are those where all of the localized spins are in the same direction. When the temperature is high, the number of possible paths is strongly reduced and the mobility becomes low because the direction of the localized spins is random. As the direction of the spins is aligned by an external magnetic field, the carrier can move freely and the mobility increases, which results in a negative magnetoresistance. Because of the additional restriction to the possible paths in the present model, the resistivity is higher in the present model than that in the one-band Hubbard model. Consequently, the resultant magnetoresistance is larger in this case than that in the Hubbard model.

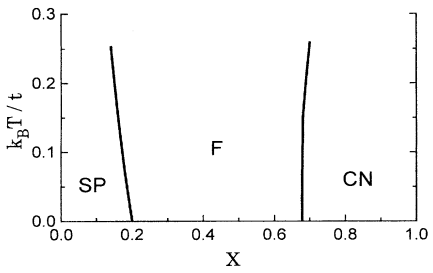

FIG. 4. Magnetic phase diagram for $(La_{1-x}X_x)MnO_3$ at low temperatures. SP, F, and CN denote the spiral, ferromagnetic, and canted states, respectively.

One of the characteristics in the GMR of Mn oxides [7] is that the value of the coefficient A is 3 or 4 times larger than that obtained in the Born approximation for, e.g., spin disorder scattering [22,23]. Our result shows that the coefficient A becomes 3.5 times larger than that in the single band Hubbard model. Thus we can conclude that the strong Hund coupling enhances the magnetoresistance effect in agreement with the experimental results.

A few possible mechanisms have been proposed so far for the GMR in $(La_{1-x}\text{-}X_x)MnO_3$. One is the formation of magnetic polarons [4] where the conductivity can be given by electron hopping of activated type between magnetic polarons [24]. In this mechanism, the condition of low carrier density is necessary to define the magnetic polaron well. The condition, however, is unlikely to be satisfied for $(La_{1-x}X_x)MnO_3$ because the GMR is observed for highly doped oxides. Recently, a mechanism of spin disorder scattering has been proposed for an explanation of the GMR in Mn oxides by Furukawa [25]. He has pointed out that A can be larger than 1 using an infinite dimension, $S \rightarrow \infty$ Kondo coupling model, and succeeded in explaining the experimental results [7]. In his theory, the value of A tends to saturate with increasing Hund coupling. Although the mechanism of resistivity in this theory seems to be different from the present one, both theories give the consistent picture that the Hund coupling plays an important role for GMR in Mn oxides.

In conclusion, we have shown, using a mean field theory, that the antiferromagnetism of $LaMnO_3$ changes to the spiral state, not the canted state, on introducing mobile carriers into the antiferromagnetic insulating phase. The canted state is shown to be favored in highly doped Mn oxides close to, e.g., $BaMnO_3$. Detailed experiments to clarify the magnetic structures in Mn oxides are desired. A possible mechanism of the giant magnetoresistance in Mn oxides has been studied in view of the strong electron correlations at high temperature. It has been shown that the dependence of the resistivity on $(M/M_s)^2$ can be enhanced by the strong Hund coupling. The tendency is in agreement with the experimental results. The temperature dependence of the resistivity and magnetoresistance are left for a future problem.

The authors thank Professor Y. Tokura for valuable discussions. A part of the present work has been done at Delft University of Technology and one of the authors (J. I.) thanks Professor G. E. W. Bauer for his kind hospitality and Murata Science Foundation for a financial support.

[1] G. Matsumoto, J. Phys. Soc. Jpn., **29**, 606 (1970).
[2] R. M. Kusters, J. Singleton, D. A. Keen, R. McGreevy, and W. Hayes, Physica (Amsterdam) **155B**, 362 (1989).
[3] R. von Helmolt, L. Haupt, K. Barner, and U. Sondermann, Solid State Commun., **82**, 693 (1992).
[4] R. von Helmolt, J. Wecker, B. Holzapfel, L. Schultz, and K. Samwer, Phys. Rev. Lett. **71**, 2331 (1993).
[5] K. Chahara, T. Ohno, M. Kasai, and Y. Kozono, Appl. Phys. Lett. **63**, 1990 (1993).
[6] M. McCormack, S. Jin, T. H. Tiefel, R. M. Fleming, J. M. Phillip, and R. Ramech, Appl. Phys. Lett. **64**, 3045 (1994).
[7] Y. Tokura, A. Urushibara, Y. Moritomo, T. Arima, A. Asamitsu, G. Kido, and N. Furukawa, J. Phys. Soc. Jpn. **63**, 3931 (1994).
[8] M. N. Baibich, J. M. Broto, A. Fert, Nguyen Van Dau, F. Petroff, P. Eitenne, G. Creuzet, A. Friederich, and J. Chazelas, Phys. Rev. Lett. **61**, 2472 (1988).
[9] Y. Tomioka, A. Asamitsu, Y. Moritomo, and Y. Tokura (to be published).
[10] Y. Tokura, Y. Taguchi, Y. Moritomo, K. Kumagai, T. Suzuki, and Y. Iye, Phys. Rev. B **48**, 14 063 (1993).
[11] T. Arima, Y. Tokura, and J. B. Torrance, Phys. Rev. B **48**, 17 006 (1993).
[12] E. O. Wollen and W. C. Koehler, Phys. Rev. **100**, 545 (1955).
[13] P.-G. de Gennes, Phys. Rev. **118**, 141 (1960).
[14] R. J. Birgeneau, Y. Endoh, K. Kakurai, Y. Hidaka, T. Murakami, M. A. Kastner, T. R. Thurston, G. Shirane, and K. Yamada, Phys. Rev. B **39**, 2868 (1989).
[15] W. Bao, C. Broholm, S. A. Carter, T. F. Rosenbaum, G. Appli, S. F. Trevino, P. Metcalf, J. M. Honig, and J. Spalek, Phys. Rev. Lett. **71**, 766 (1993).
[16] C. Zener, Phys. Rev. **82**, 403 (1951).
[17] P. W. Anderson and H. Hasegawa, Phys. Rev. **100**, 675 (1955).
[18] B. I. Shraiman and D. E. Siggia, Phys. Rev. Lett. **62**, 1564 (1989); C. Jayaprakash, H. R. Krishnamurthy, and S. Sarker, Phys. Rev. B **40**, 2610 (1989); D. Yoshioka, J. Phys. Soc. Jpn. **58**, 1516 (1989).
[19] See also, e.g., *Physics of High-Temperature Superconductivity,* edited by S. Maekawa and M. Sato (Springer-Verlag, Berlin, 1992).
[20] W. F. Brinkman and T. M. Rice, Phys. Rev. B **1**, 1324 (1970).
[21] N. Ohata and R. Kubo, J. Phys. Soc. Jpn. **28**, 1402 (1970).
[22] T. Kasuya, Prog. Theor. Phys. **16**, 58 (1956).
[23] K. Kubo and N. Ohata, J. Phys. Soc. Jpn. **33**, 21 (1972).
[24] T. Kasuya and A. Yanase, Rev. Mod. Phys. **40**, 684 (1968); Y. Shapira, S. Foner, N. F. Oliveira, Jr., and T. B. Reed, Phys. Rev. B **10**, 4765 (1974).
[25] N. Furukawa, J. Phys. Soc. Jpn. **63**, 3214 (1994).